Fragmentation- and QoT-Aware RBMSA with Spectrum Defragmentation in Dynamic Multi-Band Elastic Optical Networks

Fragmentation- and QoT-Aware RBMSA With Spectrum Defragmentation in Dynamic Multi-Band Elastic Optical Networks

Ehsan Etezadi, Farhad Arpanaei, *Member, IEEE*, Carlos Natalino, *Senior Member, IEEE*, Erik Agrell, *Fellow, IEEE*, Paolo Monti, *Senior Member, IEEE*, and Marija Furdek

***Abstract*—Multi-band elastic optical networks (MB-EONs) transmit information in multiple bands to increase the available capacity. However, they suffer from quality of transmission (QoT) degradation caused by the inter-channel stimulated Raman scattering effect, which requires addressing through tailored resource assignment. Additionally, dynamically arriving and departing optical service requests generate spectrum fragmentation (SF), where spectrum resources become scattered into non-continuous chunks and aggravate service blocking ratio (SBR) even when the total available bandwidth is sufficient. To jointly address these challenges, we propose an SF- and QoT-aware algorithm for routing, band, modulation format, and spectrum assignment (RBMSA), along with proactive spectrum defragmentation (SD), referred to as *SFQA-defrag*. The algorithm considers SF metrics and QoT levels of available channels across multiple candidate paths to ensure that the QoT requirements are met while minimizing the SF. The SD process proactively reorganizes spectrum allocation to reduce fragmentation by consolidating the spectrum gaps, which leads to lower blocking of future requests. The *SFQA-defrag* algorithm is evaluated against benchmark algorithms that independently consider either QoT or SF in three reference backbone topologies. The results demonstrate that *SFQA-defrag* significantly reduces the SBR and SF compared to benchmarks, albeit with a slight increase in the average path length.**

***Index Terms*—Multi-band elastic optical network, spectrum fragmentation, spectrum defragmentation, quality of transmission.**

I. Introduction

THE growing demand for bandwidth, driven by high-bit-rate applications such as video streaming, cloud services, and IoT, along with the continuous emergence of new services, requires dynamic and resource-efficient optical network operations [1]. This increasing demand is rapidly surpassing the capabilities of traditional C-band elastic optical networks (EONs) [2]. Multi-band elastic optical networks (MB-EONs) provide an economical way to significantly enhance data transmission capacity by utilizing multiple wavelength bands across the optical spectrum, such as L, C, S, E, O, and U bands [3]. Within each band, the optical spectrum is divided into frequency slots of fine granularity, and a channel is formed by grouping one or more contiguous slots allocated along the path carrying a modulated optical signal. Each channel is supported by a dedicated bit-rate variable transponder (BVT), which enables flexible modulation and bit rate adaptation based on the signal quality of optical connections called lightpaths. The versatility of this architecture ensures that the next-generation EON can accommodate varying traffic patterns and future growth, making it an indispensable infrastructure for enabling communication and driving innovation across industries [4]. However, the shift from conventional routing, modulation, and spectrum assignment (RMSA) in EONs to routing, band, modulation format, and spectrum assignment (RBMSA) in MB-EONs introduces additional complexity due to the necessity of choosing wavelength bands alongside paths, spectrum and modulation formats. Namely, lightpath quality of transmission (QoT) varies across wavelength bands due to nonlinear impairments. Moreover, the dynamicity in service requests leads to spectrum fragmentation (SF), where spectrum resources become fragmented into small, disjoint, and non-contiguous segments across the links [5]. A further challenge arises from the inefficient use of transceiver (TRx) capacity, especially when low-bit-rate service requests are provisioned on dedicated lightpaths, leading to underutilized spectrum resources. This can result in inefficient network capacity utilization and higher blocking probabilities for the incoming service requests. Thus, effective resource allocation strategies in MB-EONs must consider QoT and SF simultaneously. These strategies should also incorporate traffic grooming, which aggregates multiple low-bit-rate service requests onto existing lightpaths with available capacity, minimizing the need for deploying new TRxs.

To alleviate the impact of fragmentation, SF-aware RBMSA algorithms consider spectrum resource utilization and try to minimize service blocking ratio (SBR) [6]. In addition to the preemptive, SF-aware service provisioning, SF can also be addressed through spectrum defragmentation (SD) [5]. The

Received 4 September 2025; revised 16 March 2026; accepted 7 June 2026. Date of publication 11 June 2026; date of current version 25 June 2026. This work was supported by Vetenskapsrådet (2023-05249) and VINNOVA through the Celtic-Next SUSTAINET-Advance project (2025-02987). UC3M author acknowledges support from the EU-funded SEASON project (grant no. 101096120) and the TUCAN6-CM project (TEC-2024/COM-460), funded by the Community of Madrid (ORDER 5696/2024). The associate editor coordinating the review of this article and approving it for publication was Z. Zhu. *(Corresponding author: Ehsan Etezadi.)*

Ehsan Etezadi, Carlos Natalino, Erik Agrell, Paolo Monti, and Marija Furdek are with the Department of Electrical Engineering, Chalmers University of Technology, 412 96 Gothenburg, Sweden (e-mail: ehsanet@chalmers.se).

Farhad Arpanaei is with the Universidad Carlos III de Madrid, Leganes, 28911 Madrid, Spain.

Digital Object Identifier 10.1109/TNSM.2026.3702377

goal of SD is to reallocate lightpaths such that the spectral gaps are consolidated and aligned more effectively across network links, consequently allowing for the accommodation of more services and improving overall spectrum utilization. SD approaches can be categorized into two main types: reactive and proactive [7]. Reactive approaches are triggered by service-blocking events, whereas proactive approaches are executed without waiting for blocking to occur, typically by monitoring network performance metrics to determine a good timing for SD or by performing it periodically. While SD has been shown to reduce SBR, it also introduces a reconfiguration overhead, undesirable for network operators. Depending on the specific SD approach, this overhead may involve terminating, reallocating, and reestablishing selected lightpaths. The frequency of SD cycles and the number of reallocations within each cycle are key metrics used to assess the SD overhead [8]. This indicates that potential improvements in SBR and the associated overhead should be jointly considered when designing and evaluating SD approaches.

In addition to SF, another aspect to consider for resource allocation in MB-EONs is the QoT variation across the different channels and bands. This variation stems from non-linear interference (NLI), including Kerr effects and the inter-channel stimulated Raman scattering (ISRS) phenomenon, which results in self-phase modulation, cross-phase modulation, and power depletion from shorter to longer wavelengths when resources outside the C-band are used [9], [10].

QoT-aware provisioning can reduce SBR and enhance spectrum usage efficiency by assigning spectrum resources that support the highest possible modulation, based on the physical-layer quality of each channel [11]. It evaluates the QoT of predefined channels, each composed of a fixed number of frequency slots, and selects the ones offering the best transmission quality. However, this approach may inadvertently exacerbate SF. This occurs because channels with the best QoT may not always be continuous along the selected path. Also, fulfilling the requested bit rate of a service often necessitates allocating multiple non-contiguous spectrum segments, leading to several isolated channels in the same path. This issue is particularly pronounced in multi-band scenarios such as C+L+S-band networks, where differences in QoT caused by ISRS are substantial.

To address the issues mentioned above in a resource-efficient way, it is essential to balance the trade-offs between SF and QoT management in dynamic MB-EONs, and to solve the SF- and QoT-aware routing, band, modulation format, and spectrum assignment (RBMSA) problem jointly. The objective is to simultaneously reduce spectrum fragmentation, and ensure physical-layer feasibility across multiple bands. A preliminary version of this study was presented at [12], where we introduced a first heuristic algorithm for the spectrum fragmentation- and QoT-aware (SFQA) RBMSA problem in C+L+S-band dynamic MB-EONs. The algorithm considers two SF metrics along with the QoT of available channels on different candidate paths to determine the most suitable path and channel.

In this paper, we extend our previous work by introducing additional algorithmic components, refining the fragmentation modeling, and broadening the performance evaluation. The main extensions are summarized as follows:

- Integration of the original SFQA RBMSA algorithm with proactive SD, resulting in the enhanced *SFQA-defrag* framework.
- Incorporation of traffic grooming during service provisioning and traffic re-grooming during SD cycles, enabling more efficient consolidation of spectrum resources.
- Refinement of the number of cuts (NoC) fragmentation metric to more accurately capture spectrum discontinuities across neighboring links in multi-band environments.
- Adoption of a detailed physical-layer model that considers the impact of ISRS on both amplified spontaneous emission (ASE) noise and NLI, enabling accurate QoT estimation across different wavelength bands.
- Substantial expansion of the performance evaluation through extensive simulations on three real-world backbone network topologies (Japanese, USA, and Spanish networks), significantly extending the experimental validation compared to the conference version.

The results show that *SFQA-defrag* significantly decreases the SBR compared to the benchmark algorithms that consider only QoT or SF.

The rest of the paper is organized as follows. Section II reviews the state of the art for the resource management methods in dynamic MB-EONs. Section III presents the system model and physical layer assumptions. Section IV describes *SFQA-defrag*. Section V outlines the simulation settings, while Section VI evaluates the algorithm's performance. Finally, Section VII concludes the paper.

II. Related Work

The resource allocation problem in MB-EONs is particularly challenging due to the presence of physical-layer impairments, such as ISRS. Conventional RMSA techniques, primarily developed for single-band scenarios, fail to capture these additional impairments, calling for new approaches to cater for QoT requirements in MB-EONs. The RBMSA problem was first defined in [13] along with a basic generalized signal to noise ratio (GSNR)-aware provisioning strategy based on the generalized Gaussian noise model, which enables more accurate QoT estimation and efficient spectrum utilization. The impact of increased configuration granularity in next-generation BVTs was investigated in [14] by considering practical BVT implementations, and optimizing their configuration for different data rate and bandwidth combinations.

Recently, substantial research has focused on SF and its mitigation, utilizing integer linear programming (ILP) models, (meta) heuristics, and machine learning-based techniques. Proactive parallel lightpath reconfiguration in EONs was modeled as an ILP formulation in [15]. Heuristic methods for hitless bandwidth defragmentation, such as spectrum sweeping and hop tuning, were proposed in [16]. An analytical framework named AnDefrag was recently proposed to evaluate blocking probability in spectrally-spatially EONs by incorporating SD and crosstalk-avoidance constraints through a continuous-time Markov chain model [17]. Periodic SD was considered in [8], with lightpath selection for reallocation based on service parameters. A proactive SF management scheme based on crosstalk-avoided batch processing was introduced in [18], where lightpath requests are grouped within a time window to reduce fragmentation in spectrally-spatially EONs. A deep reinforcement learning-based framework was developed in [19], which jointly manages when to initiate SD, which lightpaths to reconfigure, and how to reassign spectrum resources. However, most of these studies are limited to the C band and rely on fixed reach and capacity values, primarily due to the lack of efficient, low-complexity methods for QoT estimation. To the best of our knowledge, few studies focus on fragmentation management in multi-band scenarios. Some address SF-aware service provisioning, while others explore SD in multi-band optical networks.

On the SF-aware RBMSA side, a Q-learning-based dynamic routing algorithm for C+L-band EONs, considering fiber impairments such as ISRS, was proposed in [20]. The algorithm incorporates SF effects and spectrum constraints, employing first-fit, last-fit, and exact-fit allocation strategies. Similarly, an SF- and impairment-aware RBMSA algorithm based on deep reinforcement learning was proposed in [21], where lightpaths are categorized according to their GSNR and a reward function jointly considers fragmentation reduction and physical-layer impairment caused by ISRS.

In [22], the trade-off between signal-to-noise ratio (SNR) and spectrum efficiency in C+L-band networks was addressed by proposing a resource allocation approach using C+L optical cross-connects with all-optical wavelength converters. The method minimizes link load, manages SNR impacts, and reduces SF. Similarly, a survivable RBMSA algorithm for C+L band EONs was proposed in [23], addressing ISRS, SF, and service disruptions caused by link failures.

Regarding SD, [24] presents an adaptive cross-layer bandwidth defragmentation algorithm to reduce bandwidth fragmentation arising from mismatches between services and channels in multi-band optical networks. Additionally, a signal-quality-aware proactive SD scheme for C+L-band EONs is presented in [25]. This approach minimizes SF and maintains QoT during spectrum retuning using machine learning-based QoT estimation. It incorporates nonlinear-impairment-aware SD algorithms to enhance spectrum utilization while addressing ISRS effects.

Table I summarizes the most relevant studies in the literature, specifically those addressing impairment considerations and fragmentation management in MB-EONs. To the best of our knowledge, no existing work has accounted for all impairments, including the ISRS effect in ASE and NLI noise, while simultaneously integrating SF-aware resource allocation with proactive SD. Our study addresses this gap by employing a comprehensive physical layer model that supports SF management, and QoT-aware service provisioning. In addition, we extend the analysis beyond the conventional C+L band systems considered in prior studies to include the S band, enabling performance evaluation over a broader optical spectrum.

TABLE I
LITERATURE ON RESOURCE ALLOCATION FOR MB-EONS CONSIDERING IMPAIRMENTS AND SF. **SFA**: SPECTRUM FRAGMENTATION-AWARE, **EGGN**: ENHANCED GENERALIZED GAUSSIAN NOISE, **TGR**: TRAFFICGROOMING AND RE-GROOMING

Reference	**SFA-RBMSA**	**SD**	**EGGN model**	**C+L+S-band**	**C+L-band**	**TGR**
[20]	✓	×	×	×	✓	×
[21]	✓	×	×	×	✓	×
[22]	✓	×	×	×	✓	×
[23]	✓	×	×	×	✓	×
[24]	×	✓	×	×	✓	✓
[25]	×	✓	×	×	✓	×
This study	✓	✓	✓	✓	✓	✓

III. SYSTEM MODEL AND PHYSICAL LAYER ASSUMPTIONS

In this section, we present the system model employed in this work. We outline the node functionality and network infrastructure, present the methodology used for QoT estimation, and describe the SF metrics employed in our approach. In this study, the GSNR is used as the indicator of QoT, accounting for both linear and nonlinear noise components.

A. Node and Network Architecture Model

We consider a network that comprises a set of nodes and links, representing a dynamic MB-EON scenario where service requests continuously arrive and depart. Transmission can take place in multiple bands, utilizing pre-defined channels. Each channel comprises six spectrum slots and has a total bandwidth of $6 \times 12.5 = 75$ GHz. For each service request, we must determine a path from the source to the destination node and a set of channels along that path that collectively meet the requested bit rate. Multiple channels may be allocated to a single service request depending on the needed bit rate, but they must all follow the same path. The continuity constraint dictates that the channels assigned to a particular service must be the same across all links along the chosen path. The channels do not need to be contiguous, as each channel utilizes a separate BVT. We assume a bidirectional traffic model, where the same path and modulation format support a service in both directions.

Each node in the network is equipped with C+L+S-band BVTs and reconfigurable optical add-drop multiplexers (ROADMs), enabling reconfigurable add/drop operations across multiple bands. The in-line amplifier sites are equipped with C-band erbium-doped fiber amplifiers (EDFAs) for the C-band channels, L-band EDFAs for the L-band channels, and thulium doped fiber amplifiers (TDFAs) for the S-band. The ASE-shaped noise is considered for the idle channels to guarantee the power profile consistency [26], [27]. The in-line amplifier sites are equipped with dynamic gain equalizers (DGEs) to ensure optimal launch power for each span based on the fast power optimization strategy proposed in [11].

The BVTs at each node support flexible modulation format selection and transmission rate selection based on the GSNR, soft-decision forward error correction, and variable bit rate operation [28]. This flexibility can be provided by uniform standard quadrature amplitude modulation with adaptive variable code-rate, probabilistic constellation shaping, or time-domain hybrid-format technologies [29].

The ability to vary the transmission rate at the TRx level enables traffic (re-)grooming at the optical, rather than the IP/MPLS layer. The optical layer traffic (re-)grooming is managed by an orchestrator that controls both the IP/MPLS and optical layer software defined networking (SDN) controllers. When a new request arrives, the spare capacity of the existing lightpaths between the same source and destination is utilized if sufficient; otherwise, a new lightpath must be deployed.

B. QoT Estimator

For GSNR calculation, we apply an enhanced generalized Gaussian noise (EGGN) semi-closed form model to estimate the NLI noise power, including the Kerr effects and ISRS [30], [31]. Compared to the classical GGN, EGGN model, validated through field trial experiments [32], includes an extra term that corrects for the modulation format dependence, improving the accuracy of nonlinear interference modeling. According to the concept of incoherent GN model for uncompensated optical transmission links [33], the end-to-end GSNR for a lightpath on channel i can be derived as follows:

$$GSNR^i_{\mathrm{LP}}|_{\mathrm{dB}} = 10 \cdot \log_{10}\left[\left(\Sigma_{s\in S}\sigma^s + \sigma^{-1}_{\mathrm{TRx}}\right)^{-1}\right] - \sigma_{\mathrm{Flt}}|_{\mathrm{dB}} - \sigma_{\mathrm{Ag}}|_{\mathrm{dB}}, \quad (1)$$

$$\sigma^s = \left(\frac{P^{s+1,i}_{\mathrm{tx}}}{P^{s,i}_{\mathrm{ASE}} + P^{s,i}_{\mathrm{NLI}}}\right)^{-1} \quad (2)$$

Here, $P^{s+1,i}_{\mathrm{tx}}$ is the launch power at the beginning of span $s+1$, $P^{s,i}_{\mathrm{ASE}} = n_{\mathrm{F}} h f^i (G^{s,i} - 1) R_{\mathrm{ch}}$ is noise power caused by the doped fiber amplifier (DFA) equipped with DGE, and the NLI noise power ($P^{s,i}_{\mathrm{NLI}}$) is calculated from (2) in [30]. n_{F}, h, f^i, $G^{s,i} = P^{s+1,i}_{\mathrm{tx}}/P^{s,i}_{\mathrm{rx}}$, S, and R_{ch} are the noise figure of DFA, the Planck constant, the channel frequency, the center frequency of the spectrum, the DFA gain, the set of spans, and the channel symbol rate, respectively. $P^{s,i}_{\mathrm{rx}}$ is the received power at the end of span s. σ_{TRx}, σ_{Flt}, σ_{Ag} are the transceiver SNR, the SNR penalty due to wavelength selective switches filtering, and the SNR margin due to aging.

Using 1, GSNR is calculated for any lightpath from an arbitrary source to an arbitrary destination in the network. Subsequently, for each of the K shortest paths, the highest feasible modulation format for every channel along the path is pre-calculated by comparing the estimated GSNR of each channel to the modulation format thresholds defined in the literature [4]. The pre-computed modulation format levels are used in the RBMSA process to evaluate the path–channel combinations that satisfy the required bit rate of a request, which reduces the computational overhead during service provisioning.

C. Spectrum Fragmentation (SF) Metrics

Various metrics have been proposed in the literature to quantify SF within an EON, enabling network operators to monitor and optimize spectrum resource utilization [34]. Our proposed fragmentation-aware method utilizes two key SF metrics, i.e., NoC and RSS, designed to gauge fragmentation of spectrum channels along the network links. Since the spectrum contiguity constraint is not required, as explained in Sec. III-A, we adjust these metrics to focus solely on measuring the fragmentation of channels across neighboring links. Fig. 1(a) illustrates a simple network example with four nodes, labeled $v_1 - v_4$, and five links, denoted by $e_1 - e_5$. Each link has six available channels, denoted by $c_1 - c_6$. Five active services, denoted by $d_1 - d_5$, are established in the network, and their respective channel allocation is shown in Fig. 1(b). The free spectrum is shown in white, while the color of the used resources matches the color of the corresponding demand. Note that some channels are fully occupied, while others have spare capacity available for incoming service requests. Let $b_1(c), \ldots, b_B(c)$ denote the size of the B free blocks on all links for a channel c. A free block is a set of continuous channels free on all links included in the block. The RSS metric can then be defined as follows:

$$f_{RSS}(c) = \frac{\sqrt{\sum_{i=1}^{B}(b_i(c))^2}}{\sum_{i=1}^{B} b_i(c)} \quad (3)$$

Fig. 1(c) illustrates the calculation of the RSS metric for channel c_3 as defined in (3), which has two free blocks: b_1 of size 1 (e_1) and b_2 of size 2 (e_3, e_4). NoC quantifies the SF level of a channel across the network. It is calculated per channel by assessing the occupancy state of that channel on all links in the network. The NoC for a given channel on a link is defined as the number of times the channel's state on that link differs from the state of the same channel on its adjacent links. The total NoC for a channel is then obtained by summing these values across all links. In the example shown in Fig. 1(b), no service occupies channel c_3 on link e_3. Looking at its neighbors, we see that services occupy c_3 on links e_2 and e_5 while links e_1 and e_4 have c_3 unoccupied. So, there are cuts between links e_3 and e_2, as well as links e_3 and e_5. Therefore, NoC for channel c_3 on the link e_3 is 2. The NoC value for channel c_3 on all the links can be calculated analogously, and the total NoC is obtained by summing these values, resulting in a total of 12 for this channel.

IV. SFQA-Defrag: The Spectrum Fragmentation- and QoT-Aware (SFQA) RBMSA Algorithm With Spectrum Defragmentation

In this section, we introduce the proposed algorithm for SFQA RBMSA with proactive SD in MB-EON. We start by detailing the RBMSA algorithm, followed by the description of the proactive SD algorithm, and then provide a complexity analysis to evaluate their computational cost.

A. Spectrum Fragmentation- and QoT-Aware (SFQA) RBMSA

The core idea of the *SFQA* RBMSA algorithm is to reduce the SBR by jointly considering QoT and SF during path

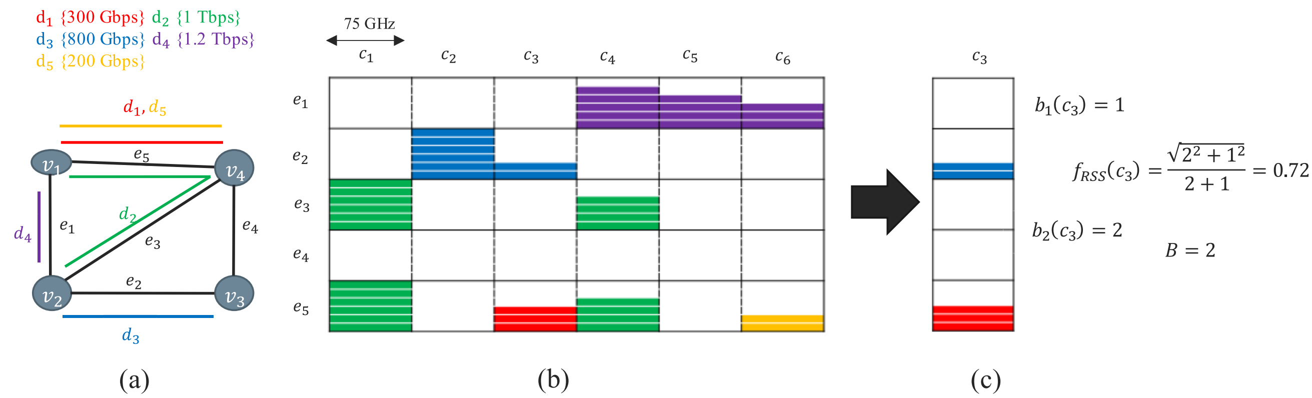

Fig. 1. An example network with four nodes and five links supporting five services (a). The spectrum occupancy state (b). Calculation of the root of sum of squares (RSS) metric value for channel 3 (c).

Algorithm 1 The spectrum fragmentation- and QoT-aware (SFQA) RBMSA

```
Input: d, P, C, M, O, S, T
Output: C_s
C_s ← ∅
br ← the bit rate of d
for each p in P do
    r ← br
    for each c in S of p do
        rc ← free capacity on channel c
        if rc > 0 then
            C_s ← C_s ∪ {c}
            r ← r − β * rc
            if r <= 0 then
                update the channel state S
                return p, C_s
    C_s ← ∅
for each p in P do
    for each c in C do
        if O(e, c) == 0 for all e in p then
            if T is RSS then
                FS(p, c) ← F_new(p, c) − F_current(p, c)
            else if T is NoC then
                FS(p, c) ← F_current(p, c) − F_new(p, c)
Sort P by descending modulation level M(p, c), then
  FS(p, c)
for each p in P do
    Sort channels on p by descending M(p, c), then
      FS(p, c)
    r ← br
    for each c in C do
        C_s ← C_s ∪ {c}
        r ← r − β * M(p, c)
        if r <= 0 then
            update channel occupancy matrix O, and state
              S
            return p, C_s
    C_s ← ∅
return C_s
```

and channel selection. For each service request, the algorithm prioritizes paths and channels that support the highest possible modulation format while also minimizing SF. The pseudocode is presented in Algorithm 1.

Inputs include the service request d, a set of candidate paths P between its source and destination nodes, the complete set of usable channels across all frequency bands $\mathcal{C}$, the pre-calculated modulation format tables M for all paths and channels, the channel occupancy matrix O, the matrix showing the remaining capacity of the established channels S, and the selected spectrum fragmentation metric T.

To illustrate these variables, an example based on the network topology in Fig. 1 is shown in Fig. 2. Fig. 2(a) shows the O matrix where 1 indicates that a channel is fully or partially occupied by a service on a link, or 0 otherwise. Fig. 2(b) shows the M table, which contains the index of the highest feasible modulation format level for K paths between each source–destination pair and for all channels. For simplicity, the example shows only the values corresponding to the shortest path of each pair. The modulation format levels in the M table range from $m = \{1, 2, 3, 4, 5, 6\}$, corresponding to bit rates from 100 Gbps to 600 Gbps. For instance, a value of 6 for a given channel means that the channel can support up to 600 Gbps. Some services may not fully utilize a channel's capacity depending on their bit rate requirements. For example, service d_3, which requires 800 Gbps, occupies the full capacity of channel c_2 and uses only 200 Gbps of channel c_3. The remaining capacity of partially used channels is tracked in the S matrix, as shown in Fig. 2(c). Each entry in the S matrix is a tuple that indicates the service request occupying the channel and the remaining capacity of the corresponding BVT on that path. In our example case, the entry $S(p_1(v_2, v_3), c_3) = (d_3, 4)$ for path $p_1(v_2, v_3)$ and channel c_3 indicates that the active BVT already used by d_3 along that path can be used to serve 400 Gbps of future incoming service requests.

The outputs of the algorithm are the selected path and a list of new channels that collectively meet the requested bit rate. If no suitable channels are found, the service request is blocked. The constraints are that all channels assigned to a service must follow the same path, and that the same set of channels must be used on every link along that path (spectrum continuity constraint).

The algorithm operates in three phases. In phase one, it checks whether the current request can be accommodated using existing channels via traffic grooming. If grooming is not successful, the algorithm proceeds to phase two where it

	c_1	c_2	c_3	c_4	c_5	c_6
e_1	0	0	0	1	1	1
e_2	0	1	1	0	0	0
e_3	1	0	0	1	0	0
e_4	0	0	0	0	0	0
e_5	1	0	1	1	0	1

(a)

	c_1	c_2	c_3	c_4	c_5	c_6
$p_1(v_1,v_2)$	6	6	6	5	4	4
$p_1(v_1,v_3)$	6	6	6	5	4	4
$p_1(v_1,v_4)$	6	6	5	4	4	3
$p_1(v_2,v_3)$	6	6	6	6	5	4
$p_1(v_2,v_4)$	6	6	5	5	5	4
$p_1(v_3,v_4)$	6	6	6	5	4	3

(b)

	c_1	c_2	c_3	c_4	c_5	c_6
$p_1(v_1,v_2)$				$(d_4,0)$	$(d_4,0)$	$(d_4,1)$
$p_1(v_1,v_3)$						
$p_1(v_1,v_4)$			$(d_1,2)$			$(d_5,1)$
$p_1(v_2,v_3)$		$(d_3,0)$	$(d_3,4)$			
$p_1(v_2,v_4)$						
$p_1(v_3,v_4)$						

(c)

Fig. 2. The channel occupancy matrix O (a), the modulation format table M (b), and the channel state S (c) for the simple network example in Fig. 1.

computes the fragmentation score (FS) for all candidate paths and available channels. Finally, in phase three, the algorithm selects a path and the corresponding channels based on the modulation format and the computed FS values. More details about each phase are provided next.

In phase one (lines 3–13), upon the arrival of service request d, the algorithm starts by analyzing all candidate paths between the source and destination nodes. For each candidate path $p \in P$, the algorithm initializes a temporary variable r with the required bit rate of the service request (line 4). It then iterates through the set of established channels along p stored in S. For each channel c, the algorithm retrieves the remaining free capacity rc and checks whether it is greater than zero (lines 6–7). If a channel has available capacity, it is added to the set of selected channels and $\beta \times rc$ is subtracted from r (lines 8–9), where β is the unit of capacity per modulation level (100 Gbps in our work). This indicates how much of the requested bit rate can be supported by reusing that channel. If there is sufficient free capacity on existing channels to accommodate the entire request, the updated value of r drops to zero or less (line 10), triggering an update in S and returning the selected path p along with the set of reused channels C_s (lines 11–12). In this process, partially utilized channels are not exclusively reserved for a single service; any remaining capacity remains available for grooming future service requests. If no path can fully accommodate the service request using existing channels, the algorithm proceeds to the second phase.

Phase two (lines 14–20) starts by identifying the free channels along each candidate path using the occupancy information from the matrix O. For each candidate channel free on all links along the path (line 16), the algorithm calculates the difference in FS obtained by assigning the channel to the service request (F_{new}), relative to the current value F_{current} (lines 17–20). If RSS is used as the metric, F_{current} and F_{new} are determined by (3). If the metric is NoC, then F_{current} and F_{new} correspond to the respective NoC values for channel c. Since low fragmentation corresponds to either a high RSS or a low NoC value, the FS must be defined differently for the two metrics to represent improvements in SF consistently. With the RSS metric, the FS is defined as $FS = F_{\text{new}} - F_{\text{current}}$, whereas with NoC, $FS = F_{\text{current}} - F_{\text{new}}$. The algorithm is designed to select the channels with the highest FS values, as they correspond to the greatest reduction of fragmentation.

Phase three (lines 21-31) identifies the best path-channel(s) combination that satisfies the service request. The list of candidate paths is sorted in the descending order of the highest supported modulation format, recorded in $M(p,c)$ (line 21). In case of ties, paths are further ranked based on the highest FS of their candidate channels. For each path in P, the available channels are then sorted in the descending order of their modulation format level, or the FS value in case of ties (line 23). The sorted channels are then iteratively selected to support the current request (lines 26–27) until the requested bit rate is fully served and r becomes zero or less (line 28). At this point, the channel occupancy matrix O is updated to reflect the new allocation. S is also adjusted to reflect the remaining free capacity on the selected channels (lines 29–30). However, if there are not enough channels along a path to meet the requested bit rate, the selected channels are cleared, and the algorithm proceeds to the next path (line 31). Should none of the paths provide sufficient channels to satisfy the request, the algorithm returns an empty set C_s, indicating that the service request d cannot be accommodated and is therefore blocked.

Fig. 3 provides an illustrative example of the *SFQA* algorithm for the network topology from Fig. 1 with two incoming service requests d_6, d_7. Two candidate paths are considered for each request. The highest supported modulation format level for each path–channel pair is shown as $M(p,c)$. The blackened parts in each channel indicate capacity that cannot be utilized due to the modulation format limitations. For example, if the modulation format level is 4, then 4 out of 6 capacity units can be used, and the remaining 2 are marked in black. It should be noted that the channel always occupies the full 75 GHz bandwidth (six contiguous frequency slots) regardless of the modulation format. The blackened portions represent reduced spectral efficiency and effective capacity, not deactivated or unused frequency slots.

When service request d_6 arrives (Fig. 3(a)), requiring 300 Gbps between nodes v_2 and v_3, the algorithm first attempts to groom the traffic by checking whether any of the established channels along the candidate paths p_1 and p_2 have sufficient free capacity. Channel c_3 on p_1, the shorter path checked first, has sufficient free capacity, allowing the service to be supported without activating a new channel. Fig. 3(b) depicts the arrival of service request d_7, requiring 400 Gbps from v_1 to v_3. While two paths are available, neither has an established channel with enough capacity to accommodate d_7. Hence, a new lightpath is needed. Channels c_1 on p_1 and c_2 and c_5 on p_2 are available. The algorithm calculates the FS for each channel based on the NoC metric, as shown on the right side of Fig. 3(b). For channel c_1 on path p_1, the fragmentation score

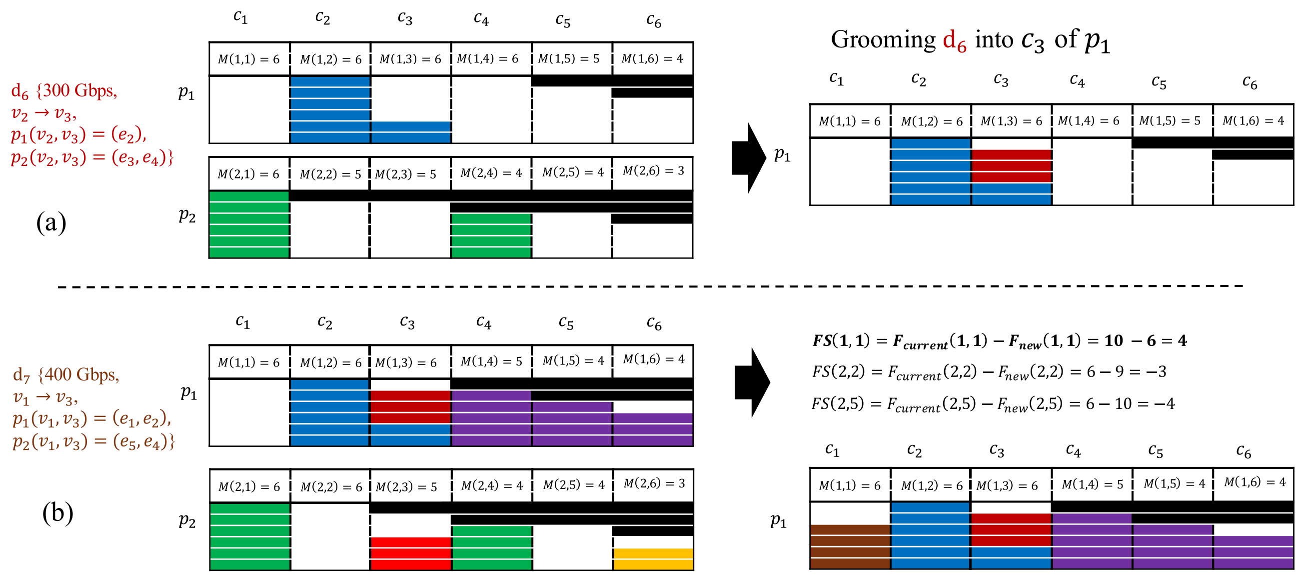

Fig. 3. An example of the SFQA algorithm provisioning a new service via traffic grooming (a), and by establishing a new lightpath (b).

is computed as $FS(1,1) = F_{\text{current}}(1,1) - F_{\text{new}}(1,1) = 4$. This score reflects the reduction in SF if c_1 is used by d_7. Among the candidates, c_1 on p_1 and c_2 on p_2 offer the same highest modulation format level, so c_1 on p_1 is selected due to its superior FS.

The proposed SD algorithm proactively initiates SD cycles, which can be triggered periodically or when a performance indicator threshold is exceeded. The pseudocode of an SD cycle of *SFQA-defrag* is presented in Algorithm 2. The main objective of the SD algorithm is to reduce spectrum fragmentation by reorganizing the channels which improve the SF most significantly. Rather than reallocating entire services, individual channels are considered for reallocation, leveraging the fact that multiple non-contiguous channels can be assigned to a single service and reallocated independently.

The algorithm receives as input the set D of active services whose channels are candidates for reallocation, the maximum number N of channels allowed for reallocation, the list of free channels $\mathcal{C}$, pre-calculated modulation format table M, the channel occupancy matrix O, the channel state matrix S, and the selected spectrum fragmentation metric T. *SFQA-defrag* comprises three phases. The aim of the first one is to re-groom traffic by consolidating partially occupied channels and freeing up resources. In the second phase, the best service channel for reallocation is identified. In the third, the algorithm seeks the best target channel to reassign the selected service channel. More details on each phase are provided next.

The first phase iterates through all active services and their associated channels. For each service channel c, it checks whether another channel c' on the same path can be re-groomed with it, based on the remaining capacity recorded in S (lines 36–38). If re-grooming is possible, the channels are consolidated and the channel c' is freed (line 39). The O and S are updated to reflect new allocations, and the counter of the number of moved service channels is incremented (lines 40–41).

B. Proactive Spectrum Defragmentation

Re-grooming is preferred because it releases resources. In contrast, channel reallocation merely relocates a channel to a position that is more favorable in terms of SF. If the number of moved service channels reaches the maximum allowable limit N, the algorithm stops (lines 42–43). Otherwise, it moves to the next phase.

The second phase identifies the best candidate channels for reallocation and stores them in the set DO, initially empty (line 44). To this end, the defragmentation score (DS) is calculated only for fully occupied channels, avoiding unnecessary movement of partially utilized channels that could accommodate additional services (lines 45–47). DS is computed by hypothetically removing the channel and computing the difference in the SF metric before F_{current} and after removal F_{removed} (lines 48–51). The definition of DS depends on the selected SF metric. If RSS is used, higher values indicate lower fragmentation and the score is computed as $F_{\text{removed}} - F_{\text{current}}$. A positive value means that removing the channel leads to an increase in RSS, and thus, a decrease in SF. In contrast, when NoC is used, lower values indicate lower fragmentation and the score is calculated as $F_{\text{current}} - F_{\text{removed}}$. A positive value in this case implies a reduction in SF. Channels with a positive DS value whose removal reduces fragmentation are added to DO, along with their corresponding service and the calculated score (lines 52–53). The list is sorted in descending order of the DS values, so that the channels whose removal offers the highest potential improvement in SF are ranked first (line 54).

The third phase selects the best target channel to which the selected candidates from DO will be reallocated. It begins by initializing two variables: RS_{best}, which keeps track of the best SF improvement score found, and c_{target}, which stores the corresponding target channel (lines 55–56). For each candidate channel in DO, the algorithm considers free channels that use

Algorithm 2 The spectrum defragmentation (SD) Cycle

Input: D, N, $\mathcal{C}$, M, O, S
33 $MovedCount \leftarrow 0$;
34 $D_s \leftarrow \varnothing$; `// service selected for reallocation`
35 **for** *each* d *in* D **do**
36   **for** *each* c *used by* d **do**
37   **for** *each* $c' \in \mathcal{C},\ c' \neq c$ **do**
38   **if** $S(p_d, c')[2] \neq 0$ ***and*** $S(p_d, c)[2] + S(p_d, c')[2] \leq M(p_d, c)$ **then**
39   **Re-groom** channels c and c';
40   **Update** O, S;
41         $MovedCount \leftarrow MovedCount + 1$;
42   **if** $MovedCount \geq N$ **then**
43   **break** ; `// Stop if the maximum allowed movements are reached`
44 $DO \leftarrow \varnothing$;
45 **for** *each* d *in* D **do**
46   **for** *each* c *in channels of* d **do**
47   **if** c *is fully occupied by* d **then**
48   **if** T *is* RSS **then**
49         $DS(p_d, c) \leftarrow F_{\text{removed}}(p_d, c) - F_{\text{current}}(p_d, c)$
50   **else if** T *is* NoC **then**
51         $DS(p_d, c) \leftarrow F_{\text{current}}(p_d, c) - F_{\text{removed}}(p_d, c)$
52   **if** $DS(p_d, c) > 0$ **then**
53         $DO \leftarrow DO \cup (c, d, DS(p_d, c))$
54 Sort DO by descending $DS(p, c)$,
55 $RS_{\text{best}} \leftarrow 0$;
56 $c_{\text{target}} \leftarrow \varnothing$;
57 **for** *each* $(c, d, DS(p_d, c))$ *in* DO **do**
58   **for** *each* c' *in* $\mathcal{C}$ **do**
59   **if** $O(e, c') == 0$ *for all* e *in* p_d **then**
60   **if** $M(p_d, c') >= M(p_d, c)$ **then**
61   **if** T *is* RSS **then**
62           $RS(p_d, c') \leftarrow F_{\text{new}}(p_d, c') - F_{\text{current}}(p_d, c')$
63   **else if** T *is* NoC **then**
64           $RS(p_d, c') \leftarrow F_{\text{current}}(p_d, c') - F_{\text{new}}(p_d, c')$
65   **if** $RS(p_d, c') > RS_{best}$ **then**
66           $RS_{\text{best}} \leftarrow RS_d(i)$
67           $c_{\text{target}} \leftarrow c'$
68   **if** $RS_{best} \geq -1 \cdot DS(p_d, c)$ **then**
69   **move** channel c to c_{target}
70   **update** O, S
71     $MovedCount \leftarrow MovedCount + 1$;
72   **if** $MovedCount \geq N$ **then**
73   **break**

the same path and can support the same modulation format as possible target channels (lines 57–60). Reallocation score RS is calculated for each eligible target channel to measure the change in SF if it replaced the original channel. The value of RS is equal to the difference in the SF metric before and after a hypothetical change from the original to the target channel. Depending on the chosen SF metric, the algorithm selects the reallocation option that yields either a higher value (for RSS) or a lower value (for NoC) (lines 61–64). The RS value for the current target channel is compared to the highest score found so far (line 65) and the best target channel, denoted as c_{target}, is updated if the new RS value is better (lines 66–67).

After evaluating RS for all available target channels and identifying the best option, the algorithm compares the RS with the DS of the candidate channel (line 68). This comparison determines whether channel reallocation would yield a benefit in terms of the SF metric. If there is a gain in the SF metric, the selected channel c is reallocated to the target channel c_{target}. The counter for the number of moved service channels is incremented, and the channel occupancy (O) and channel state (S) matrices are updated (lines 69–71). The algorithm continues until the maximum number of allowed reallocated service channels, N, is reached, at which point the SD cycle terminates (lines 72–73).

In the proposed *SFQA-defrag* algorithm, channel reallocations are performed only when they lead to an improvement in the selected fragmentation metric. Therefore, by construction, every accepted defragmentation action guarantees a non-degradation of the fragmentation state. Given the theoretical relationship between fragmentation and blocking [35], [36], the algorithm steers the network toward operating regimes with reduced blocking probability.

Fig. 4 illustrates an example of an SD cycle based on the network state shown in Fig. 1, after accommodating service requests d_6 and d_7 (Fig. 3). In the first phase, the algorithm scans all active services and their corresponding channels to identify candidates for traffic re-grooming. Services d_5 and d_1 share the same path, and channel c_3 has sufficient capacity to accommodate d_5. Consequently, the service channel of d_5 is consolidated to channel c_3. As a result, the original service channel of c_6 is released (Fig. 4(a)). In the second phase, the algorithm identifies candidates for reallocation (Fig. 4(b)). For simplicity, only channels c_4 and c_5 of service d_4 are considered in this example. The DS value is computed for these channels based on the NoC metric. As a result, c_5 is selected for reallocation due to the higher DS value (denoted in bold). In the third phase, the algorithm searches for the best target channel along the path of d_4, considering free channels that support the modulation format of c_5. Channels c_2 and c_3 meet these criteria. For each candidate target channel, the algorithm calculates RS, as shown on the right side of Fig. 4(b). The RS is computed based on the NoC metric, ultimately selecting c_3 as the target channel. Although the resulting allocation may appear more fragmented in the figure due to the non-adjacent channel positions, it does not increase SF in our model. This is because the contiguity constraint is not enforced, and only the continuity constraint is considered.

C. Complexity Analysis

In the worst-case scenario, when phase 1 of the *SFQA* algorithm fails to accommodate the incoming request through grooming, the algorithm proceeds to evaluate all path–channel combinations. This includes checking the modulation format level from the M look-up table and sorting the available channels for each of the $|P|$ candidate paths. The total time complexity can be expressed as $T_{\text{SFQA}} = O(|P||\text{S}|) + O(|P||\mathcal{C}|) + O(|P||\mathcal{C}| \log |\mathcal{C}|)$, which simplifies to $T_{\text{SFQA}} = O(|P||\mathcal{C}| \log |\mathcal{C}|)$ by considering $\max |\text{S}| = |\mathcal{C}|$.

The worst-case time complexity of an SD cycle, assuming no N-based early termination, can be expressed as $T_{\text{SD}} = O(|D|\,\mathcal{C}_d) + O(|D|\,\mathcal{C}_d) + O(|D|\,\mathcal{C}_d \log(|D|\,\mathcal{C}_d)) + O(|D|\,\mathcal{C}_d\,|\mathcal{C}|)$, where $|D|$ is the number of demands and $\mathcal{C}_d$

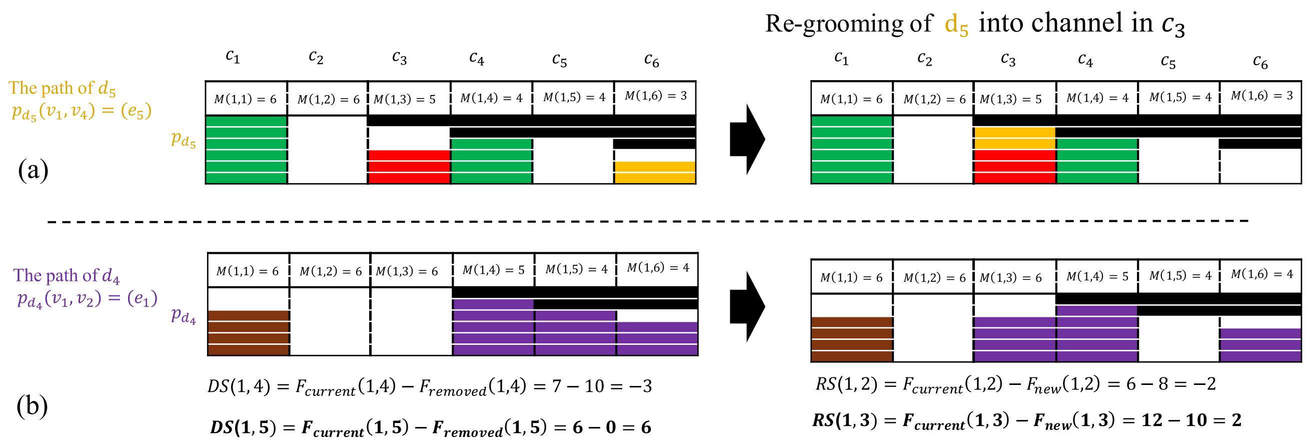

Fig. 4. An example of defragmentation done via traffic re-grooming (a), and by reallocating a service channel (b).

the number of channels per demand. Noting that $\mathcal{C}_d \leq |\mathcal{C}|$, this simplifies to $T_{\text{SD}} = O(|D|\,|\mathcal{C}|^2)$.

Despite these worst-case bounds, both *SFQA* and *SFQA-defrag* maintain lightweight computational complexity, making them suitable for real-time spectrum reallocation in dynamic MB-EON environments.

V. Simulation Settings

We consider C+L+S-band EONs with a total bandwidth of 20 THz, distributed as 6 THz for the C-band, 6 THz for the L-band, and 8 THz for the S-band, divided into 268 channels, each occupying 75 GHz (6 × 12.5 GHz). A 400 GHz guard band is maintained between adjacent bands. Standard single-mode fiber with a zero-water peak is assumed, and spectrum continuity constraint is enforced. Simulations are conducted on three topologies: the Japanese (JPN) (12 nodes and 17 links), the United States (US) topology (14 nodes and 22 links), and the Spanish (SPN) topology (30 nodes and 56 links) [11]. The maximum span length is set to 80 km. We consider six modulation formats, from PM-BPSK to PM-64QAM, operating at 64 Gbaud, with supported bit rates ranging from 100 Gbps (PM-BPSK) to 600 Gbps (PM-64QAM). We use $\beta = 100$ Gbps, corresponding to the modulation level granularity. EDFAs with noise figures of 4.5 dB and 5 dB are used for the C- and L-bands, respectively, and a TDFA with a 6 dB noise figure for the S-band.

Service requests are characterized by randomly generated end nodes, with uniform distribution, and bit-rates uniformly distributed between 50 Gbps and 600 Gbps, with a granularity of 50 Gbps. Service request arrivals follow a Poisson process with an average arrival rate of $\lambda = 25$ requests per time unit. Service holding time has a negative exponential distribution with an average of $1/\mu$ time units. Consequently, the offered traffic load is expressed as λ/μ normalized traffic units (NTUs). Given that the average bit-rate of a single request is 325 Gbit/s, a traffic load of 100 NTUs corresponds to approximately 32.5 Tbps of offered traffic load. The load is adjusted to achieve a SBR between 0.01% and 1% for the proposed *SFQA-defrag* algorithm. It is important to note that variations in the results are expected due to the inherent stochastic nature of the Poisson process. Hence, we conduct simulations of the proposed algorithms using 10 different seeds for the random number generator of the network environment to ensure robustness of the numerical results. Each simulation run processes two million service requests, followed by a calculation of the confidence interval to quantify the level of uncertainty in the results. We consider $K = 3$ pre-computed shortest paths. Additional experiments with $K = 5$ showed only marginal performance improvements while increasing the computational complexity. Therefore, $K = 3$ is used as a practical trade-off between performance and computational overhead.

We implement the proposed *SFQA* algorithm within the Optical RL-Gym framework [37] and consider two SF metrics. The version that uses the NoC metric is denoted as *SFQA-NoC*, while the version using the RSS metric is denoted as *SFQA-RSS*. Analogously, *SFQA-defrag-NoC* applies NoC in RBMSA and SD processes, while *SFQA-defrag-RSS* uses RSS. The SD period is set to 10 service request arrivals, with a maximum of $N = 10$ allowed reallocations for proactive SD, in an effort to balance the SBR gain and the SD overhead [8].

To evaluate the performance of the proposed algorithm, we compare it with three benchmark algorithms that are well-established in the literature: QoT-aware *QA*, which considers only the QoT of the channels during resource assignment [11]; and fragmentation-aware *FA-NoC* and *FA-RSS*, which rely solely on the NoC and RSS fragmentation metrics, respectively, and represent standard fragmentation-aware resource allocation strategies from the literature [38], [39], [40]. In addition, we include the shortest available path *SAP* algorithm, a baseline approach that selects the shortest path and the channel that supports the highest efficient modulation format along that path. For all methods, when identical candidate modulation formats or SF metric values are identified, channels with the lowest frequency are prioritized.

VI. Numerical Results

Figure 5 shows the SBR for the tested strategies under different offered traffic loads for the JPN, US, and SPN topologies. The *SFQA* algorithm, which jointly considers

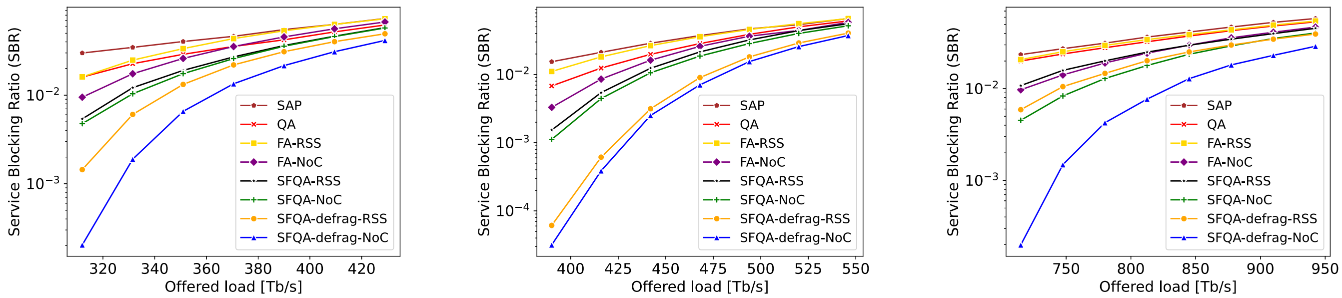

(a) JPN topology (b) US topology (c) SPN topology

Fig. 5. The service blocking ratio (SBR) for the three network topologies.

TABLE II
SPECTRUM DEFRAGMENTATION (SD) OVERHEAD FOR THREE NETWORK TOPOLOGIES

Topology	Number of reallocations		Number of completed SD cycles	
	SFQA-defrag-RSS	SFQA-defrag-NoC	SFQA-defrag-RSS	SFQA-defrag-NoC
JPN topology	39	24	9.6	8.3
US topology	77	56	9.9	9.7
SPN topology	17	19	7.2	7.6

QoT and SF, achieves performance superior to all benchmark algorithms. When differentiated metric-wise, the *SFQA-NoC* algorithm slightly outperforms *SFQA-RSS*. It significantly surpasses *QA* and *FA-NoC*, reducing the blocking ratio by 23% and 22% on average over all traffic loads in the JPN topology. A similar trend is observed for the US topology, where *SFQA-NoC* has by 28% and 19% average lower blocking ratio than *QA* and *FA-NoC*, performing close to *SFQA-RSS*. However, in the SPN topology, *SFQA-NoC* outperforms *SFQA-RSS* by 22%. Additionally, in the SPN topology, *SFQA-NoC* outperforms the *QA* and *FA-NoC* algorithms by 39% and 22%, respectively. The superior performance of the *SFQA* algorithms over *QA* highlights the benefits of incorporating occupancy state information into the path and channel selection processes. Also, jointly considering both QoT and SF metrics leads to more informed routing and allocation decisions, resulting in improved resource utilization compared to strategies that focus on only one aspect. At a 95% confidence level, the confidence intervals of the SBR results for *SFQA-NoC* are 1.4%, 1.7%, and 1.5% for the JPN, US, and SPN topologies, respectively.

When comparing the *SFQA-defrag-RSS* and *SFQA-defrag-NoC* algorithms to their *SFQA-NoC* and *SFQA-RSS* counterparts, we observe improvement of 41.2% and 20%, respectively, for the JPN topology. The improvements are analogous for the US (43% and 41%) and the SPN topology (44% and 18%). It is important to note that SD introduces additional overhead in terms of the number of reallocations and completed SD cycles, which are crucial factors in evaluating SD algorithms. Table II shows the average number of channel reallocations and completed SD cycles for the three network topologies over all the loads. The performance gains of *SFQA-defrag-NoC* come at the cost of an average of 8.5 completed SD cycles and 33 reallocations per 100 arrivals across all topologies. The numbers for *SFQA-defrag-RSS* become 8.7 SD completed cycles and 44 reallocations. Given that we start one SD cycle upon each 10 service request arrivals and allow at most $N = 10$ reallocations per cycle, the theoretical maximum number of SD cycles per 100 arrivals is 10, resulting in potentially 100 total reallocations. However, these limits are never reached regardless of the topology. The number of SD cycles and reallocations depends on specific network characteristics, such as path diversity and link distribution, which influence the level of fragmentation and modulation format of the channels. These factors affect how often reallocation opportunities arise and how effective they are in reducing SF.

Joint consideration of the reduction in the SBR (Fig. 5) and the incurred SD overhead (Table II) provides useful insight into the performance of the proposed algorithms when they consider the two different metrics. In the JPN topology, *SFQA-defrag-NoC* obtains 29% lower blocking than *SFQA-defrag-RSS*, while reallocating 38% fewer connections in 13% lower number of SD cycles. In the US topology, *SFQA-defrag-NoC* has 4% lower blocking, reallocates 27% fewer connections and completes 2% fewer SD cycles. In the SPN topology, *SFQA-defrag-NoC* blocks 46% less requests, while reallocating only 10% more connections in 5% more SD cycles than *SFQA-defrag-RSS*. These results indicate that using NoC as metric leads to solutions with lower service request blocking ratios at a lower SD overhead.

Figure 6 shows the average GSNR levels across different scenarios for the topologies under exam. Since paths are not changed during the reallocation process in *SFQA-defrag*, their GSNR levels are close to those of the corresponding *SFQA* algorithms and are therefore not shown in the figure. Among all algorithms, *QA* achieves the highest GSNR, surpassing the *SFQA* variants by 1%, 0.5%, and 4% for the JPN, US, and SPN topologies, respectively. However, this advantage in terms of signal quality does not translate into better

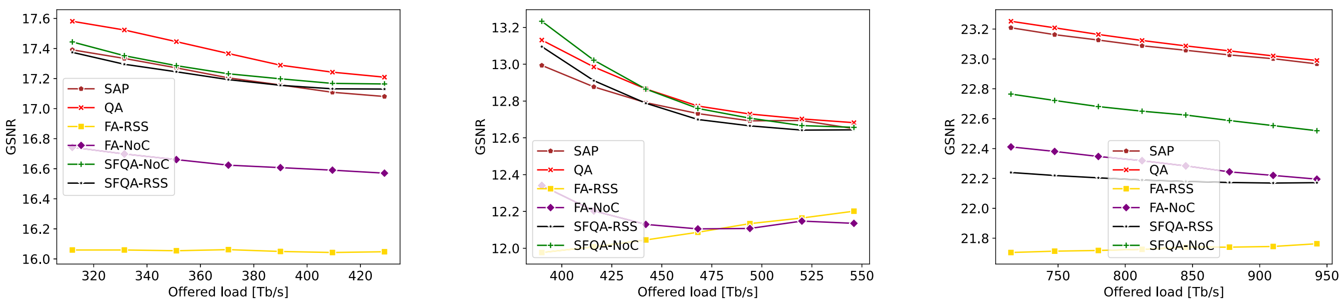

(a) JPN topology (b) US topology (c) SPN topology

Fig. 6. The average generalized signal to noise ratio (GSNR) for the three network topologies.

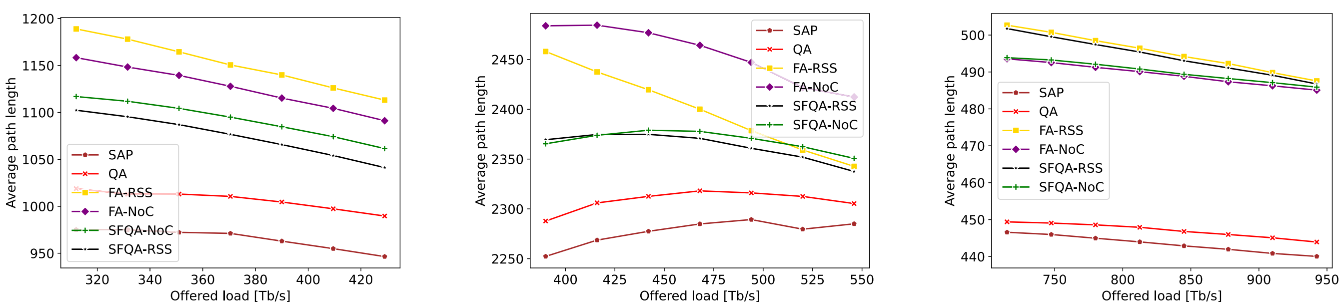

(a) JPN topology (b) US topology (c) SPN topology

Fig. 7. The average path length for the three network topologies.

performance in terms of SBR. On the contrary, the SBR results from Fig. 5 show that the *SFQA* algorithms significantly outperform *QA*. This observation highlights the importance of incorporating occupancy state and SF information into the routing and spectrum allocation process, rather than relying solely on physical-layer quality parameters. As expected, the worst GSNR levels are observed for *FA-NoC* and *FA-RSS*, which only consider fragmentation and disregard QoT of the channels.

Figure 7 shows the average path lengths obtained by the different approaches for the considered topologies. The advantages of *SFQA* in terms of the SBR come at the cost of longer paths. The *SFQA-NoC* algorithm uses on average 8% and 13% longer paths than the *QA* and *SAP* algorithms for the JPN topology, 2% and 4% longer for the US topology, and 9% and 10% longer for the SPN topology. This behavior arises because *SFQA* prioritizes SF reduction when selecting paths and channels. As a result, it may favor routes that offer better spectrum availability, ultimately lowering the SBR. As expected, the *SAP* algorithm performs best in this metric, as it prioritizes shorter path lengths over other metrics.

VII. Conclusion

This paper presents a heuristic algorithm for QoT- and spectrum fragmentation-aware RBMSA in multi-band elastic optical networks. By integrating physical-layer modeling with spectrum occupancy information quantified with two different fragmentation metrics (NoC and RSS), our approach reduces the service blocking ratio by up to 39% compared to the QoT-aware benchmarking algorithm and by up to 22% compared to a fragmentation-aware benchmark. This improvement comes with a modest increase of 2-13% in the average path length. The addition of proactive spectrum defragmentation obtains a further 44% reduction in the blocking ratio, which comes with a defragmentation overhead of 33 channel reallocations and 8.5 completed defragmentation cycles per 100 request arrivals on average. These results demonstrate that jointly considering physical-layer quality indicators and spectrum occupancy information during resource allocation leads to higher spectrum resource usage efficiency in multi-band elastic optical networks.

References

[1] P. A. Baziana, "Optical data center networking: A comprehensive review on traffic, switching, bandwidth allocation, and challenges," *IEEE Access*, vol. 12, pp. 186413–186444, 2024.

[2] W. Klaus, P. J. Winzer, and K. Nakajima, "The role of parallelism in the evolution of optical fiber communication systems," *Proc. IEEE*, vol. 110, no. 11, pp. 1619–1654, Nov. 2022.

[3] T. Hoshida et al., "Ultrawideband systems and networks: Beyond C + L-band," *Proc. IEEE*, vol. 110, no. 11, pp. 1725–1741, Nov. 2022.

[4] F. Arpanaei et al., "Enabling seamless migration of optical metro-urban networks to the multi-band: Unveiling a cutting-edge 6D planning tool for the 6G era," *J. Opt. Commun. Netw.*, vol. 16, no. 4, pp. 463–480, 2024.

[5] B. C. Chatterjee, S. Ba, and E. Oki, "Fragmentation problems and management approaches in elastic optical networks: A survey," *IEEE Commun. Surveys Tuts.*, vol. 20, no. 1, pp. 183–210, 1st Quart., 2018.

[6] B. Bao et al., "SDFA: A service-driven fragmentation-aware resource allocation in elastic optical networks," *IEEE Trans. Netw. Service Manage.*, vol. 19, no. 1, pp. 353–365, Mar. 2022.

[7] R. Wang and B. Mukherjee, "Provisioning in elastic optical networks with non-disruptive defragmentation," *J. Lightw. Technol.*, vol. 31, no. 15, pp. 2491–2500, Aug. 15, 2013.

[8] J. Comellas, L. Vicario, and G. Junyent, "Proactive defragmentation in elastic optical networks under dynamic load conditions," *Photonic Netw. Commun.*, vol. 36, no. 1, pp. 26–34, Aug. 2018.

[9] P. Poggiolini, "A generalized GN-model closed-form formula," 2018, *arXiv:1810.06545*.

[10] D. Semrau, R. I. Killey, and P. Bayvel, "A closed-form approximation of the Gaussian noise model in the presence of inter-channel stimulated Raman scattering," *J. Lightw. Technol.*, vol. 37, no. 9, pp. 1924–1936, May 15, 2019.

[11] F. Arpanaei et al., "Synergizing hyper-accelerated power optimization and wavelength-dependent QoT-aware cross-layer design in next-generation multi-band EONs," 2024, *arXiv:2411.02911*.

[12] E. Etezadi et al., "Joint fragmentation- and QoT-aware RBMSA in dynamic multi-band elastic optical networks," in *Proc. 24th Int. Conf. Transparent Opt. Netw. (ICTON)*, Jul. 2024, pp. 1–5.

[13] N. Sambo et al., "Provisioning in multi-band optical networks," *J. Lightw. Technol.*, vol. 38, no. 9, pp. 2598–2605, May 15, 2020.

[14] J. Müller et al., "Physical-layer-aware multi-band optical network planning framework for rate-adaptive transceivers," *J. Opt. Commun. Netw.*, vol. 16, no. 5, pp. B71–B80, 2024.

[15] M. Zhang, C. You, and Z. Zhu, "On the parallelization of spectrum defragmentation reconfigurations in elastic optical networks," *IEEE/ACM Trans. Netw.*, vol. 24, no. 5, pp. 2819–2833, Oct. 2016.

[16] M. Zhang, Y. Yin, R. Proietti, Z. Zhu, and S. J. B. Yoo, "Spectrum defragmentation algorithms for elastic optical networks using hitless spectrum retuning techniques," in *Proc. Opt. Fiber Commun. Conf. Expo. Nat. Fiber Optic Eng. Conf. (OFC/NFOEC)*, Mar. 2013, pp. 1–3.

[17] I. Ahmed, E. Oki, and B. Chand Chatterjee, "AnDefrag: Analytical model for blocking probabilities considering defragmentation in spectrally-spatially elastic optical networks," *IEEE Trans. Netw.*, vol. 33, no. 4, pp. 1528–1542, Aug. 2025.

[18] B. C. Chatterjee, A. Wadud, and E. Oki, "Proactive fragmentation management scheme based on crosstalk-avoided batch processing for spectrally-spatially elastic optical networks," *IEEE J. Sel. Areas Commun.*, vol. 39, no. 9, pp. 2719–2733, Sep. 2021.

[19] E. Etezadi et al., "Deep reinforcement learning for proactive spectrum defragmentation in elastic optical networks," *J. Opt. Commun. Netw.*, vol. 15, no. 10, p. E86, 2023.

[20] J. L. Ravipudi et al., "Impairment-and fragmentation-aware dynamic routing, modulation and spectrum allocation in C+L band elastic optical networks using Q-learning," *Opt. Switching Netw.*, vol. 47, Feb. 2023, Art. no. 100717.

[21] D. Yan, N. Feng, J. Lv, D. Ren, J. Hu, and J. Zhao, "DRL-based fragmentation-and impairment-aware resource allocation algorithm in C+L band elastic optical networks," *Opt. Fiber Technol.*, vol. 90, Mar. 2025, Art. no. 104133.

[22] Y. Teng et al., "SRS-proactive-aware resource allocation based on all-optical wavelength converters in C+L band optical networks," *J. Lightw. Technol.*, vol. 42, no. 19, pp. 6632–6646, Oct. 15, 2024.

[23] Y. Liu, N. Feng, L. Shen, J. Lv, D. Yan, and J. Zhao, "Fragmentation and ISRS-aware survivable routing, band, modulation, and spectrum allocation algorithm in multi-band elastic optical networks," *Appl. Sci.*, vol. 14, no. 11, p. 4755, May 2024.

[24] J. Liu, Z. Xi, and R. Gu, "Adaptive cross-layer bandwidth defragmentation for multi-band optical network," in *Proc. Asia Commun. Photon. Conf./Int. Photon. Optoelectronics Meetings (ACP/POEM)*, Nov. 2023, pp. 1–5.

[25] R. K. Jana et al., "Machine learning-assisted nonlinear-impairment-aware proactive defragmentation for C+L band elastic optical networks," *J. Opt. Commun. Netw.*, vol. 14, no. 3, pp. 56–68, Mar. 2022.

[26] F. Arpanaei et al., "Launch power optimization for dynamic elastic optical networks over C+L bands," in *Proc. Int. Conf. Opt. Netw. Design Model. (ONDM)*, Coimbra, Portugal, 2023, pp. 1–3.

[27] V. Curri, "Multiband optical transport: A cost-effective and seamless increase of network capacity," in *Proc. OSA Adv. Photon. Congr.*, 2021, Art. no. NeTu2C.3, doi: 10.1364/NETWORKS.2021.NeTu2C.3.

[28] Infinera Blog. *What the Heck Are Modem SNR and Holistic Co-Design*. Accessed: Apr. 2024. [Online]. Available: https://www.infinera.com/blog/what-the-heck-are-modem-snr-and-holistic-co-design/tag/optical/

[29] J. Cho and P. J. Winzer, "Probabilistic constellation shaping for optical fiber communications," *J. Lightw. Technol.*, vol. 37, no. 6, pp. 1590–1607, Mar. 15, 2019.

[30] P. Poggiolini and M. Ranjbar-Zefreh, "Closed form expressions of the nonlinear interference for UWB systems," in *Proc. Eur. Conf. Opt. Commun. (ECOC)*, Sep. 2022, pp. 1–4.

[31] M. R. Zefreh et al., "A GN-model closed-form formula supporting ultra-low fiber loss and short fiber spans," 2021, *arXiv:2111.04584*.

[32] Y. Jiang et al., "Experimental test of closed-form EGN model over C+L bands," in *Proc. Eur. Conf. Opt. Commun. (ECOC)*, vol. 2023, 2023, pp. 254–257.

[33] P. Poggiolini, G. Bosco, A. Carena, V. Curri, Y. Jiang, and F. Forghieri, "The GN-model of fiber non-linear propagation and its applications," *J. Lightw. Technol.*, vol. 32, no. 4, pp. 694–721, Feb. 15, 2014.

[34] M. Quagliotti, D. C. Arango, M. Schiano, A. Carena, M. Cantono, and V. Curri, "Spectrum fragmentation metrics and their use in optical channel allocation algorithms," in *Proc. 19th Italian Nat. Conf. Photonic Technol. (Fotonica)*, Jun. 2017, pp. 1–4.

[35] W. Shi, Z. Zhu, M. Zhang, and N. Ansari, "On the effect of bandwidth fragmentation on blocking probability in elastic optical networks," *IEEE Trans. Commun.*, vol. 61, no. 7, pp. 2970–2978, Jul. 2013.

[36] L. Al-Tarawneh and S. Taebi, "Minimizing blocking probability in elastic optical networks by varying the bandwidth granularity based on optical path fragmentation," *Photonics*, vol. 4, no. 2, p. 20, Mar. 2017.

[37] C. Natalino et al., "Optical networking gym: An open-source toolkit for resource assignment problems in optical networks," *J. Opt. Commun. Netw.*, vol. 16, no. 12, pp. G40–G51, 2024.

[38] Y. Yin, M. Zhang, Z. Zhu, and S. J. B. Yoo, "Fragmentation-aware routing, modulation and spectrum assignment algorithms in elastic optical networks," in *Proc. Opt. Fiber Commun. Conf. Exposit. Nat. Fiber Optic Eng. Conf. (OFC/NFOEC)*, Mar. 2013, pp. 1–3.

[39] M. Shimoda and T. Tanaka, "Mask RSA: End-to-end reinforcement learning-based routing and spectrum assignment in elastic optical networks," in *Proc. Eur. Conf. Opt. Commun. (ECOC)*, Sep. 2021, pp. 1–4.

[40] P. Lechowicz, M. Tornatore, A. Włodarczyk, and K. Walkowiak, "Fragmentation metrics in spectrally-spatially flexible optical networks," in *Proc. ONDM*, 2020, pp. 235–247.